COBEM 2023 27TH INTERNATIONAL CONGRESS OF MECHANICAL ENGENEERING

ABCM Brazilian Society of Mechanical Sciences and Engineering
27th ABCM International Congress of Mechanical Engineering
December 04-08, 2023, Florianópolis-SC, Brazil

COB-2023-0307
Modeling, Simulation and Dynamic Analysis of Roller Bearing with Surface Damage

Lucas Florentino Varella
Aline de Almeida Soares
Flavio Yukio Watanabe
Mechanical Engineering Departament, Federal University of São Carlos, Rodovia Washington Luis, km 235 - São Carlos - SP - BR CEP: 13565-905
varella.lf@hotmail.com, alineas@ufscar.br, fywatanabe@ufscar.br

Abstract. *Rolling bearing failures are frequent in the routine operation of industrial equipments. These failures often occur unexpectedly, causing unscheduled interruption in production and, consequently, losses. One way to inspect the development of these failures is through predictive analysis of equipment such as sensitive inspection, boroscopy, lubricant analysis, thermography and vibration analysis, the latter being frequently used in monitoring the rating life of the equipment. Finding a mathematical model that provides understanding of how bearing failure evolves is very useful, therefore, through the analysis of the vibration spectrum, the severity of the failure in the component can be understood and maintenance can be scheduled in advance. This study presents the dynamic simulation of a faulty roller bearing mathematical model with 2 degrees of freedom for evaluating the behavior of the response in time and frequency, comparing a healthy and a roller bearing with surface damage. The mathematical model was implemented in the Octave software and the results obtained in numerical simulation were compared with the literature results. The impacts on the frequency response were evaluated by varying theses parameters: number of rolling elements, length and depth of the defect and the load applied to the roller bearing.*

Keywords: *Rolling bearing, Vibration, Maintenance, Wear.*

1. INTRODUCTION

Rolling bearings are widely used in industrial machines and their selection process is based on operation conditions, such as loads directions and intensities, rotation speed, running accuracy and noise levels, as well on the required service life and reliability. However, despite careful design and selection, some of these bearings fail before reaching the required service life, generally causing damages, maintenance need, productivity drop and economic losses. It is estimated that 10 billion rolling bearings are manufactured around the world, every year, and about 9,5% of these bearings are replaced preventively prior to failure, and 0,5% are replaced because they failed or are damaged, mainly due to surface fatigue, lubrication problems, contamination, and improper handling, mounting, or loading conditions (SKF, 2017). The early detection of bearing damage enables a scheduled maintenance, avoiding undesirable and costly unscheduled machine downtime due to bearing failure. Monitoring machine elements health allows the adoption of predictive techniques such as lubricant analysis, thermography and noise and vibration analysis (SKF, 2017).

Damages in rolling surfaces of bearing elements generally occur due to rolling contact wear or fatigue, plastic deformation and debris particles mixed into the lubricant (Halme and Andersson, 2010). The international standard 15243 (ISO, 2017) classifies the rolling bearings damage and failures modes that occur while the bearing is installed in the machine and during operation. The ISO failure modes are divided into six categories: rolling contact fatigue, wear, corrosion, electrical erosion, plastic deformation, and fracture/cracking. Figure 1 illustrates the failure modes classified into subcategories (SKF, 2017).

When a surface defect is formed in a rolling bearing element, its contact with another surface generates an impact force, resulting in an impulsive response of the others bearing elements and the application of vibration analysis techniques allows the identification of its origin and severity stage (Saruhan *et al.*, 2014). Figure 2 illustrates how the evolution of a rolling bearing surface defect affects the global vibration level along time and how different professional condition monitoring instruments and technologies may define a pre-warning time, before sensorial failure detection and a catastrophic failure. Additionally, Figure 2 presents an example of bearing inner ring damage progress, associated with each six damage stages (SKF, 2017)).

Tandon and Choudhury (1999) show that vibration responses measurement allows the use of different methods for detection and diagnosis the rolling bearing defects in time and frequency domains. Vibration in the time domain can be analyzed through overall RMS level, crest factor, probability density, kurtosis and shock pulse method. On the other hand, the vibration analysis in the frequency domain is based on the application of Fourier transform concepts, implemented

Figure 1. Failure modes of rolling bearing (SKF, 2017). (Images courtesy of SKF).

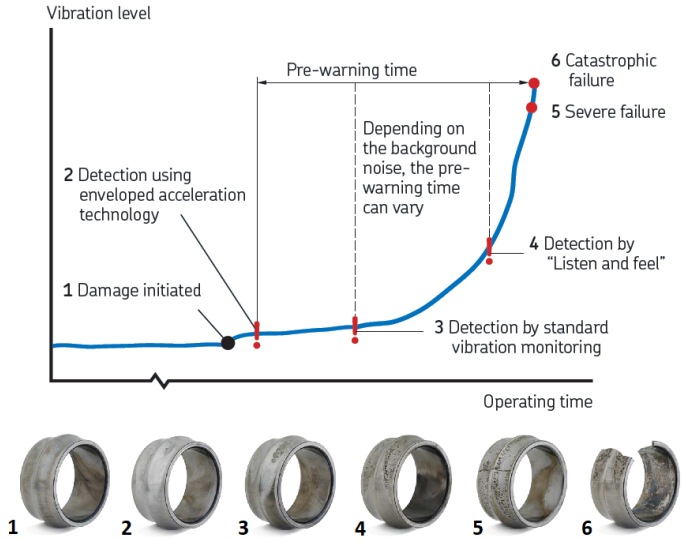

Figure 2. Vibration level associated to rolling bearing damage evolution (SKF, 2017). (Images courtesy of SKF).

through FFT (Fast Fourier Transform) algorithms and the spectral analysis allow the identification of the defect location and its severity state, but may not indicate the defect at the initial stage.

The complexity of the loading and failure mechanisms of rolling bearings leads to development of theoretical and experimental investigations of the influence of different parameters on bearing wear and damage phenomena (Shao *et al.*, 2013); (Cong *et al.*, 2013); (Wang *et al.*, 2015); (Mishra *et al.*, 2017); (Zhang *et al.*, 2020). Dynamic models of rotor-bearing systems with different number of degrees of freedom (DOF) were developed to simulate bearing surface defects of different types and size. Shao *et al.* (2013) adopted a 2-DOF dynamic model for a cylindrical roller bearing with a localized surface defect on its races and considering both the time-varying deflection excitation and the time-varying contact stiffness excitation produced by the defect. Mishra *et al.* (2017) applied a 5-DOF model of a ball bearing considering the effects due to preload and normal force due to ball race contact. Zhang *et al.* (2020) considered a 4-DOF dynamic system model with different compound fault in a deep groove ball bearing and investigate the influences of coupling excitation and time-varying displacement excitation.

For numerical and experimental purposes, the surface damages in rolling bearings are usually modeled as discontinuities in the bearing races (inner or outer) or in the rolling element (sphere or roller). Figure 3 shows three different models of surface damages in the outer race of a rolling bearing. In damages type A and B, rolling element does not touch the bottom of the defect in the bearing race, but it is possible that this occurs for defect type C, depending on its width. Furthermore, the surface damages may affect the local stiffness contact of rolling elements and races and it and can be numerically modeled using the finite element method (Shao *et al.*, 2013).

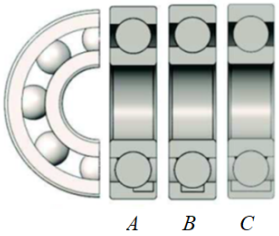

Figure 3. Types of surface damages in the outer race of a rolling bearing.

Another important factor to be considered for the study of failures in bearings are the internal clearance resulting from the preload assembly, thermal expansion effects or due to the usual wear of the bearings (Harris, 2006). In the present study, a 2-DOF roller bearing mathematical model was adopted and the developed dynamic simulation results allows the behavior analysis of the responses in time and frequency domains, comparing a healthy and a roller bearing with a surface damage in the outer race.

2. MATHEMATICAL MODELING

This chapter presents the equation of a bearing subject to a force and which is in a condition of wear. The proposed modeling considers that the set has two degrees of freedom.

2.1 Rolling bearigs and mean caracteristics

The versatility of roller bearings in motion transmission enables their use in simple and complex mechanical systems. This type of bearing consists of its inner and outer raceways, cage and rolling elements.The mains geometric caracteristics of roller bearings are diameter of rolling element (D), pitch diameter (d), diameter of inner raceway(d_i), diameter of outer raceway(d_e), radius of cage $(r = d/2)$, radius of inner receway $(r_i = d_i/2)$ and radius of outer receway $(r_e = d_e/2)$, as show on Fig. 4(a) and 2(b) . Two surfaces, as inner raceway and roller element or outer raceway and roller element, are in contact by pure rolling or rolling in combination with sliding, favoring the appearance of surface failure, known as surface fatigue (Norton, 2013).

Contact stresses in a roller bearing are estimated from Hertz contact theory, described in Eq. (1). The load distribuit on rolling elements (Q) depends on the external load (F),quantite of rolling bearings (z), radial clearance (C_r), displacement between both raceways (δ), as show in Figure 1(c) and 1(c) (Harris, 2006).

Considering a cylindrical roller bearing, the load distributed on its contacts can be written as in Fig. 4(c).

$$Q = k\delta^{10/9} \tag{1}$$

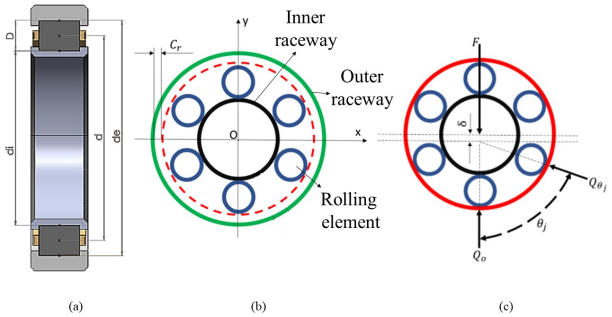

Figure 4. (a) and (b) Geometric caracteristics of a roller bearings. (c) Load applied on roller bearing.

2.2 Roller passing frequency

Bearing failures can occur in any of its components (rolling elements, cage, inner or outer raceway). The frequency of failure is associated with the speed of rotation of each componentes. According to Bezerra (2004) the cage speed (V_g) can be obtained by the arithmetic average between the speed rotation of the outer (V_o) and inner (V_i) raceway. Therfore, relating from Eq. (2) to Eq. (5), it is possible to obtain de frequency of cage Eq. (6). Considering (f_i) and (f_o) frequency

of inner and outer raceway,respectively.

$$V_g = \frac{(V_i + V_e)}{2} \quad , \tag{2}$$

$$f_g = \frac{V_g}{r} \quad , \tag{3}$$

$$V_i = f_i \, r_i \quad , \tag{4}$$

$$V_e = f_e \, r_e \quad , \tag{5}$$

$$f_g = \frac{f_i r_i \; + f_e r_e}{d} \quad , \tag{6}$$

The roller passing frequency of inner is the relationship between rolling elements and this raceway. The equation describe this phenomenon is:

$$f_{ci} = |f_g - f_i| \, z \quad , \tag{7}$$

Similarly, the passing frequency of outer is the relationship between rolling elements and this raceway. The equation describe this phenomenon is:

$$f_{ce} = |f_g - f_e| \, z \qquad , \tag{8}$$

2.3 Equation of moviment for set shaft-rolling bearing

The mathematical model used to describe the bearing motion equations are based on Shao *et al.* (2013) and Sunnersjo (1977), which consider the components of this machine element an association of masses, springs and dampers. For this work, it is considered that the deformation of the shaft is the same as that of the rolling elements. Therefore, the equation of motion of the set is described in Eq. (9). Since m and c are total mass and damping of shaft and roller bearing, Q is the load distruited in each rolling element, and F is the radial force applied to the roller bearing, as show in Fig. 4(c).

$$m\ddot{x} + c\dot{x} + \sum_{j=1}^{z} Q = F \quad , \tag{9}$$

Replacing Eq. (1) into Eq. (9), and considering the stiffness (K) is constant.

$$m\ddot{x} + c\dot{x} + K\sum_{j=1}^{z} \delta_j^{2/3} = F \quad , \tag{10}$$

The total radial deformation (δ_j) is relationship between the diametral clearence (C_r) and their rolling elements in both direction x and y. This relationship is described according to Sunnersjo (1977) in Eq. (11):

$$\delta_j = x\cos(\theta) + ysen(\theta) - C_r \quad , \tag{11}$$

The bearing fault (H_d) is inserted into the equation of motion as an addition to the diametral clearance (C_r), as show in Fig. 5. The fault is a conbitation of length $(\Delta\theta_d)$ and depth (H_d).

Therefore, equation described the roller bearing with flaut in both direction x and y is:

$$m\ddot{x} + c\dot{x} + K\sum_{j=1}^{z} \beta_j \left[\cos(\theta_j) + ysin(\theta_j) - (C_r + H_d)\right]^n \cos(\theta_j) = F_x \quad , \tag{12}$$

$$m\ddot{x} + c\dot{x} + K\sum_{j=1}^{z} \beta_j \left[\cos(\theta_j) + ysin(\theta_j) - (C_r + H_d)\right]^n \sin(\theta_j) = F_x \quad , \tag{13}$$

In order to numerically exclude possible negative loadings, the (β) function has the following relation:

$$\beta_j = \left\{ \begin{array}{l} 1 \; for \; \delta_j > 0 \\ 0 \; for \; \delta_j < 0 \end{array} \right\} \tag{14}$$

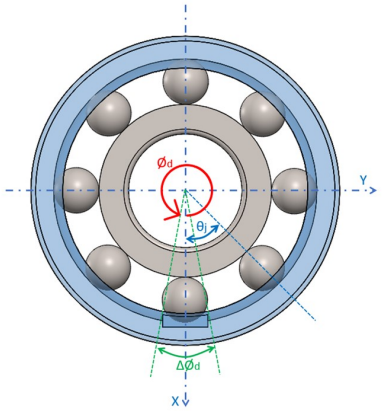

Figure 5. Representation the fault on roller bearing.

2.4 Computational implementation

The purpose of this section is to prepare the equations, described by Eq. (11) and cto be computationally solved. Thus, the system of second-order differential equations is rewritten into first-order equations. For this transformation, the state-space math tool is used. Considering the following substitutions:

$$\{q_1 = x;\ q_2 = \dot{x};\ \dot{q_1} = q_2;\ \dot{q_2} = \ddot{x} \tag{15}$$

$$\{q_3 = y;\ q_4 = \dot{y};\ \dot{q_3} = q_4;\ \dot{q_4} = \ddot{y} \tag{16}$$

Replacing Eq. (15) and (17) into Eq. (12) and (13):

$$m\dot{q_2} + cq_2 + K\sum_{j=1}^{z} \beta_j \left[q_1 \cos\theta_j + q_3 sen\theta_j\right]^{10/9} cos\theta_j = F_x \tag{17}$$

$$m\dot{q_4} + cq_4 + K\sum_{j=1}^{z} \beta_j \left[q_1 \cos\theta_j + q_3 sen\theta_j\right]^{10/9} sen\theta_j = F_y \tag{18}$$

Therefore, the Eq. (17) and (18) can be rewritten as:

$$\begin{Bmatrix} \dot{q_1} \\ \dot{q_2} \\ \dot{q_3} \\ \dot{q_4} \end{Bmatrix} = \begin{Bmatrix} q_2 \\ (-cq_2 - K\delta_{jx} + F_x)\,\frac{1}{m} \\ q_4 \\ (-cq_4 - K\delta_{jy} + F_y)\,\frac{1}{m} \end{Bmatrix} \tag{19}$$

The computational implementation of the system of equations presented in this section is described in Fig. 6.

3. RESULTS

After reviewing the concepts and understanding the computational implementation, test runs were performed with functions with known responses for a healthy and a defective rolling bearing and subsequently parameter variations were tested in order to understand the level of sensitivity present in the developed model. The parameters number of rolling elements, defect length and defect depth were varied.

For all the complete time response graphs presented below it will be possible to notice a decay in the value of the amplitudes until reaching a region of stability. This region is characterized as a transient region of the numerical solution and is related to how the implemented routine finds the solution of the problem and should not be confused with the transient of the physical system. The amplitude values presented were all evaluated after this region, that is, in the stability region of the response where it was in the steady state.

For both the testing part and the sensitivity analysis of the variables the initial input parameters are the same and are presented in Figure 7. All parameter values were taken from Shao *et al.* (2013).

3.1 Rolling bearing without surface defect

For the first understanding if the response in time and frequency were presented in the expected way, sine and cosine functions with known period and a bearing without defect were used so that:

$$F_x = 480\cos\left(f_i t\right) \tag{20}$$

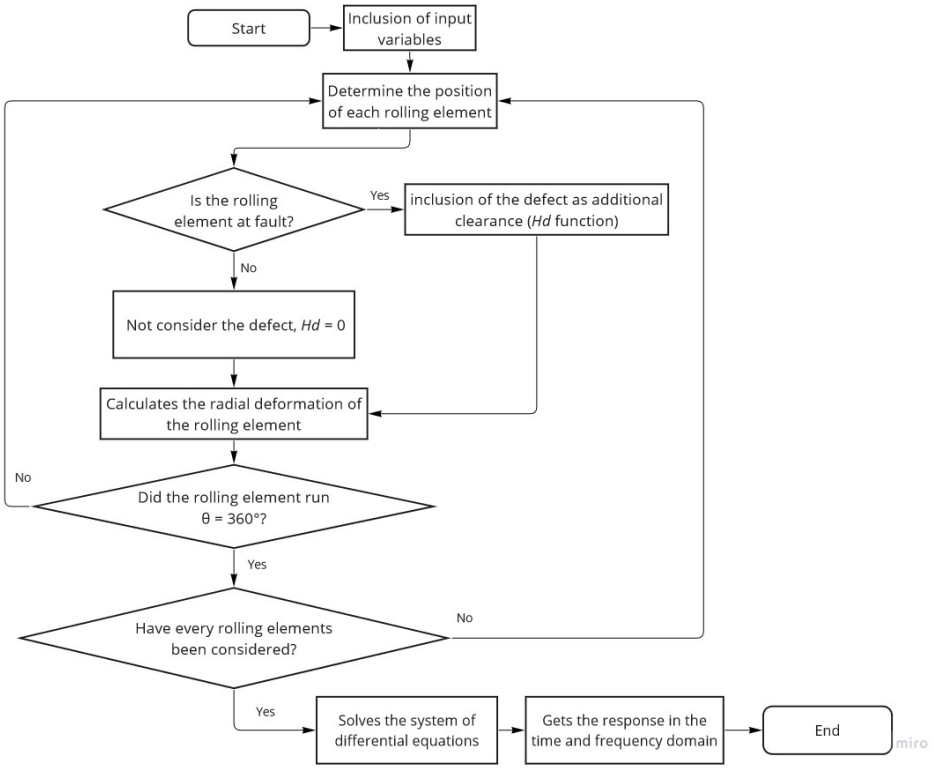

Figure 6. Flowchart of the computational implementation.

Variable	Description of variable	Value		Variable	Description of variable	Value
c	Damping coeficient	350 Ns/m		n	Expoent related to geometry of rolling element	10/9
m	Equivalent set mass	3 kg		d	Pitch diameter	5.15x10^{-2} m
K	Equivalent Stiffness	1.50x10 (N/m)		D	Diameter of rolling element	1.10 x10^{-2} m
z	Number of roller elements	12		d_i	Diameter of inner raceway	4.05 x10^{-2} m
C_r	Diametral clearence	0 m		d_e	Diameter of outer raceway	6.25 x10^{-2} m

Figure 7. Parameter values used in non-defective bearing operation tests

$$F_y = 480 \sin(f_i t) \tag{21}$$

As input rotation was established $f_i = 4000\ rpm$, so it is expected as response perfectly equal sinusoids only lagged $\pi/2$ radians and the frequency spectrum showing peaks at 66.67 Hz. In Figure 8 it is possible to notice that the curves have the same profile, they leave the indicated initial condition of 10^{-6} m, they are offset by $\pi/2$ radians and have a frequency of 66.67 Hz, as expected for 4000 rpm.

3.2 Bearing with surface defect and unbalance

Subsequently, it was studied how the inclusion of a surface defect in the bearing could influence the shape of both the time response and the frequency spectrum response. At that moment, an input corresponding to a concentrated static loading equiavalent to 480 N and an unbalance force was implemented. The equation for x and y is shown by the equations below:

$$F_x = 480 + 480 \cos(f_i t) \tag{22}$$

$$F_y = 480 + 480 \sin(f_i t) \tag{23}$$

In Figure 9, unlike the response in time without defect, we observe peaks highlighted mainly in the curve referring to the displacement in x. These peaks can be interpreted as the passage of the rolling elements over the defect.

In Figure 10 the frequencies $f_i = 66,67$ and $f_{ce} = 314\ Hz$ stand out confirming the expected behavior for the surface defect and an unbalance with $f_i = 4000\ rpm$, Z = 12 elements and inner race with 0 rpm as showed in Eq. 8. Due to the parameters implemented and the model used being a reduced two degrees of freedom model the response that will be

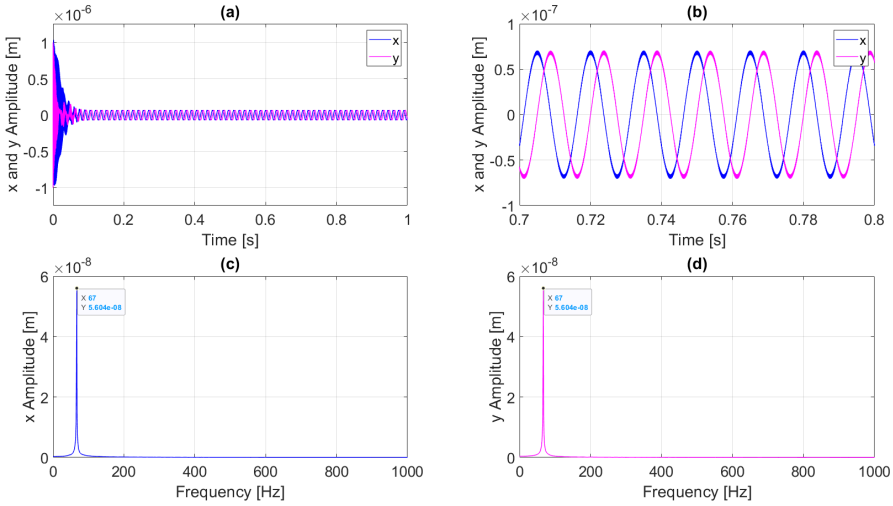

Figure 8. Time and frequency spectrum response for a bearing without surface defects.

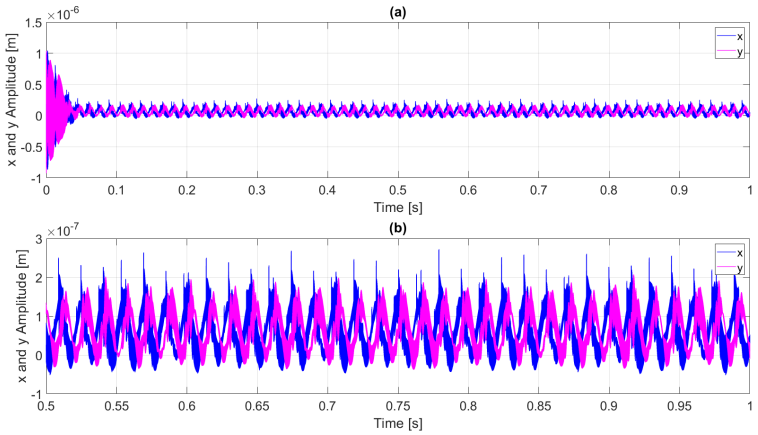

Figure 9. Time response for rolling bearings with surface defect and unbalance.

seen will be that of the outer race of the bearing, this being a ratio between the frequency of the cage and the number of rolling elements.

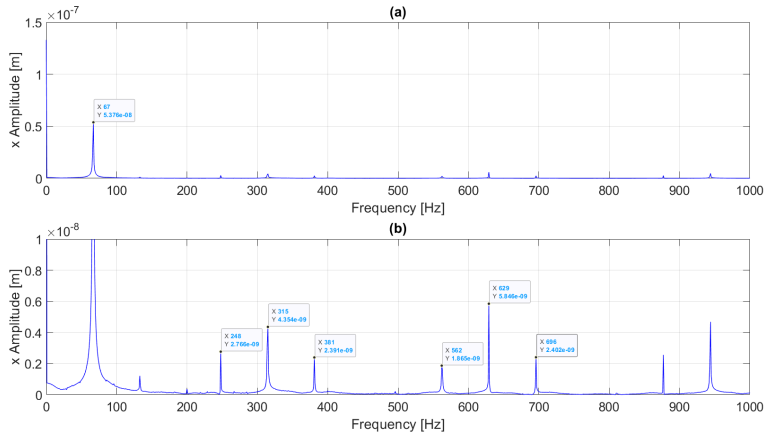

Figure 10. Frequency spectrum for rolling bearings with surface defect and unbalance.

3.3 Varying number of rolling elements

One way to understand the level of sensitivity of the implemented model is to vary some specific parameters and evaluate the system response. At first, the number of rolling elements was varied in such a way that it was possible to evaluate its amplitude in meters according to the number of rolling elements. The equations used are equations 22 and 23 and the number of rolling elements is given the values of 8, 9, 10, 11 and 12 elements. It is expected that the higher the number of rolling elements, the better the load distribution, the lower the efforts and the lower the amplitude presented in the response. An important detail is that the failure frequency of the outer race varies proportionally with the number of rolling elements, so it is expected that the lower the number of rolling elements, the higher the amplitude and the lower the failure frequency. We can observe this result in Figure 11.

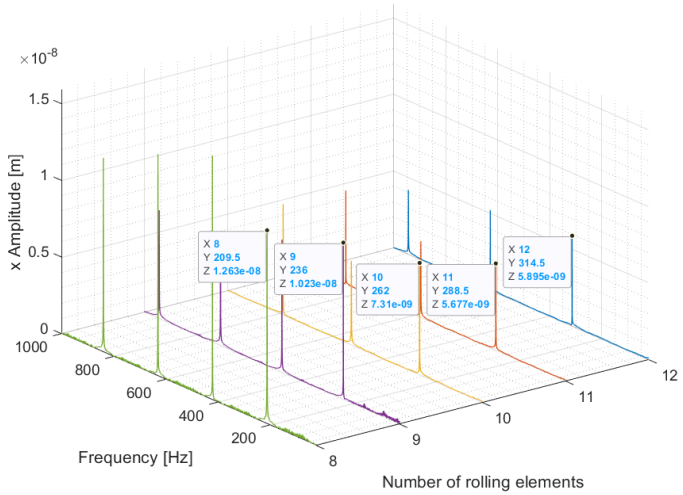

Figure 11. Waterfall plot of the variation of the amplitude with the variation of the number of rolling elements.

Another way to see how the model understands the increase and decrease in the number of rolling elements is presented in Figure 12 (a) and (b), where we can see how with the increase in the number of rolling elements there is a decrease in the amplitude of the response both in displacement and acceleration.

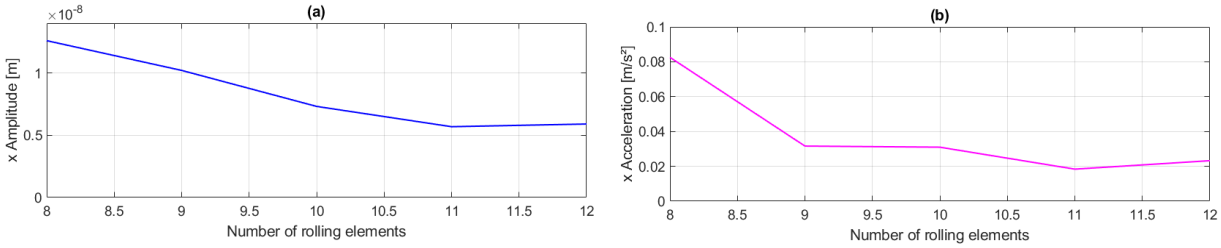

Figure 12. Line chart of the variation of the amplitude with the variation of the number of rolling elements.

3.4 Varying defect length

Subsequently, the response due to variation in defect length was evaluated. The greater the defect length, measured in degrees, it is expected to be higher vibration amplitude seen in the response. In this case, the failure frequency evidenced does not change, because the defect length was changed, but the number of rolling elements always remained Z = 12 elements. The equations used are equations 22 and 23 and the defect length is given the values of 1, 2, 3, 4 and 5 degrees. In Figure 13 it is possible to clearly notice that the frequency does not change and that there is an evident growth of the vibration amplitude with the increase of the defect size.

It is possible to notice in Figure 14 (a) and (b) that by increasing the defect size the amplitude in both displacement and acceleration also increases, and it is possible to visualize in another way the increase in amplitude with increasing defect length.

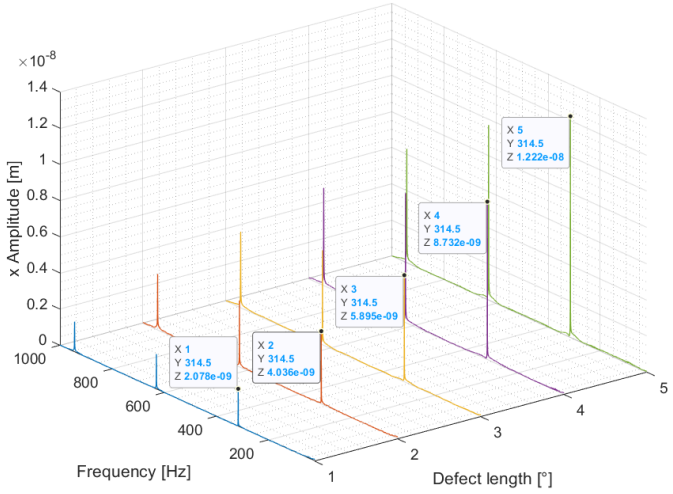

Figure 13. Waterfall plot of the variation of the amplitude with the variation of the defect length.

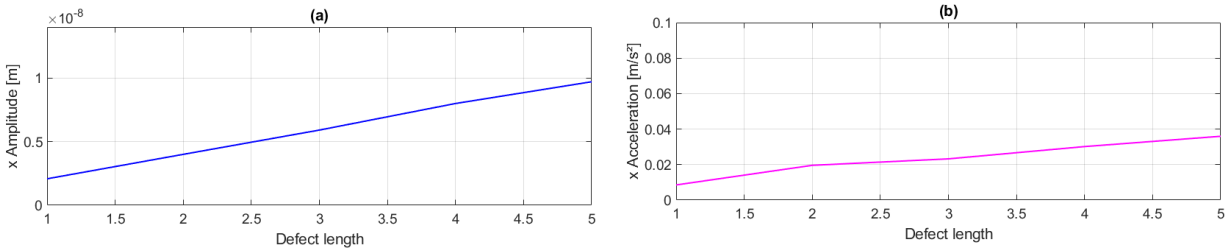

Figure 14. Line chart of the variation of the amplitude with the variation of the defect length.

3.5 Varying the defect depth

Finally, the variation of the defect depth and the response of the amplitude values were evaluated. Unlike what was found for the other parameters, regardless of the variation of their value the amplitudes found remained constant, both for displacement and acceleration and do not show an increasing trend as expected, as can be seen in Figure 15.

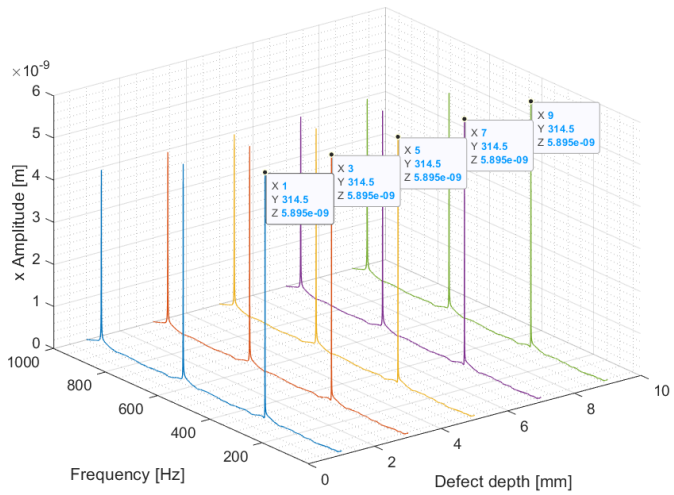

Figure 15. Waterfall plot of the variation of the amplitude with the variation of the defect depth.

One way to interpret this limitation of the model is related to the stiffness of the system. In the model used the stiffness of the system remains constant regardless of the variation of the parameters, which in reality does not occur. When the

depth of the defect increases, naturally the local stiffness changes, decreasing its value and providing an increase in the value of the amplitudes. In more complex models this type of approach is taken into account and consequently ends up providing an increase in amplitudes with increasing defect depth, but even so, the variation found is small, demonstrating that for this type of analysis a very sensitive model must be implemented. Although the sensitivity is not as expected, the defect is inserted in the bearing and it is possible to verify this by observing that the failure frequency of 314.5 Hz stands out in all analyzes.

4. CONCLUSION

The math modeling of 2 DOF applied to cylindrical roller bearing possilited to observe the influence of some parameters, as number of rolling bearing, and the characteristics of defaults, as depth and witdth. Draw up a model that includes the variation of the stiffness of the set in the different moments of the passage of the rolling element through the defect, evaluate this variation in a finite element software, increase the number of degrees of freedom of the model, use another approach for the modeling of the defect where it is possible for the rolling element to touch the bottom of the defect and elaborate a comparison with experimental tests are suggestions for future work.

5. REFERENCES

Bezerra, R.d., 2004. *Detecção de Falhas em Rolamentos por Análise de Vibração*. Master's thesis, Faculdade de Engenharia Mecânica, Universidade Estadual de Campinas, Campinas, Brasil.

Cong, F., Chen, J., Dong, G. and Pecht, M., 2013. "Vibration model of rolling element bearings in a rotor-bearing system for fault diagnosis". *Journal of Sound and Vibration*, Vol. 332, pp. 2081–2097.

Halme, J. and Andersson, P., 2010. "Rolling contact fatigue and wear fundamentals for rolling bearing diagnostics - state of the art". *Part J: Journal of Engineering Tribology*, Vol. 224, pp. 377– 393.

Harris, T.A., 2006. *Rolling Bearing Analysis*. Taylor and Francis Group, New York.

ISO, 2017. *ISO 15243: Rolling bearings - Damage and failures - Terms, characteristics and causes*. ISO.

Mishra, C., Samantaray, A.K. and Chakraborty, G., 2017. "Ball bearing defect models: A study of simulated and experimental fault signatures". *Journal of Sound and Vibration*, Vol. 400, pp. 86–112.

Norton, R., 2013. *Projeto de máquinas: uma abordagem integrada*. Bookman, Porto Alegre.

Saruhan, H., Sandemir, S., Çiçek and Uygur, I., 2014. "Vibration analysis of rolling element bearings defects". *Journal of Applied Research and Technology*, Vol. 12, pp. 384–395.

Shao, Y., Liu, J. and Ye, J., 2013. "A new method to model a localized surface defect in a cylindrical roller-bearing dynamic simulation". *Journal of Engineering Tribology*, Vol. 228, pp. 140–159.

SKF, 2017. *Bearing damage and failure analysis*. SKF Group.

Sunnersjo, C.S., 1977. *Rolling Bearing Vibrations: The effects of varying compliance, manufacturing, tolerances and wear*. Ph.D. thesis, Faculty of Engineering, University of Aston, Birmingham, England.

Tandon, N. and Choudhury, A., 1999. "A review of vibration and acoustic measurement methods for the detection of defects in rolling element bearings". *Tribology International*, Vol. 32, pp. 469–480.

Wang, F., Jing, M., Dong, G., Liu, H. and Ji, B., 2015. "Dynamic modelling for vibration analysis of a cylindrical roller bearing due to localized defects on raceways". *Proceedings of the Institution of Mechanical Engineers, Part K: Journal of Multi-body Dynamics*, Vol. 229, pp. 39–64.

Zhang, X., Yan, C., Liu, Y., Yan, P., Wang, Y. and Wu, L., 2020. "Dynamic modeling and analysis of rolling bearing with compound fault on raceway and rolling element". *Shock and Vibration*, Vol. Article ID 8861899, p. 16.

6. RESPONSIBILITY NOTICE

The following text, properly adapted to the number of authors, must be included in the last section of the paper:
The author(s) is (are) solely responsible for the printed material included in this paper.